Mon. Not. R. astr. Soc. (1991) **248,** 424–438

Non-Gaussian initial conditions in cosmological *N*-body simulations – II. Cold Dark Matter models

L. Moscardini[1,3], S. Matarrese[2], F. Lucchin[4] and A. Messina[1]

[1]*Dipartimento di Astronomia, Università di Bologna, via Zamboni 33, I-40126 Bologna, Italy*
[2]*Dipartimento di Fisica G. Galilei, Università di Padova, via Marzolo 8, I-35131 Padova, Italy*
[3]*Astronomy Centre, University of Sussex, Falmer, Brighton BN1 9QH*
[4]*Dipartimento di Astronomia, Università di Padova, Vicolo dell'Osservatorio 5, I-35122 Padova, Italy*

Accepted 1990 August 12. Received 1990 August 1

SUMMARY

Results are reported on *N*-body simulations of the large-scale structure of the Universe starting from non-Gaussian initial conditions in a Cold Dark Matter cosmogony. We consider three *multiplicative* models where the peculiar gravitational potential is obtained by performing a non-linear transformation on a Gaussian random field: while keeping the standard form for the initial power spectrum, this procedure provides highly non-random phases. The resulting distributions in space and velocity are analysed by different statistical tests and compared with the evolution of a standard Gaussian model with the same initial amplitude. We find that both the clustering dynamics and the present texture are mostly sensitive to the sign of the initial skewness of mass fluctuations. In particular, models characterized by a substantial predominance of primordial underdense regions (negative skewness) evolve towards a *cellular* structure with large correlation length and enhanced peculiar motions. Our results suggest that the Cold Dark Matter scenario can succeed in reproducing structures on large scales if the random-phase hypothesis is abandoned.

1 INTRODUCTION

The model for the formation of cosmic structures which has been most thoroughly investigated is the standard Cold Dark Matter (hereafter CDM) scenario; this is based on the following assumptions: (i) the Universe has density parameter $\Omega_0 = 1$ and vanishing cosmological constant; (ii) the primordial power spectrum of adiabatic fluctuations is scale invariant (Harrison–Peebles–Zel'dovich hypothesis); (iii) the statistics of initial perturbations is Gaussian. Such a specific choice is motivated by the prediction of the typical inflationary model. The two most important parameters of this scenario are the value of the Hubble constant, $H_0 = 100\ h$ km s^{-1} Mpc^{-1}, and the bias parameter b, defined as the square root of the ratio between the variance of galaxy counts and the mass variance in a sphere of radius $8\ h^{-1}$ Mpc. While the former quantity, which is allowed to vary in a restricted range, mainly affects the perturbation-transfer function, the latter fixes the amplitude of primordial fluctuations. A bias factor $b > 1$ naturally enhances the number and the size of filamentary structures and voids in the galaxy distribution in better agreement with observations (White *et al.* 1987). A third parameter, the amount of baryonic material Ω_b, with a value in the range allowed by the standard nucleosynthesis model, does not greatly affect the scenario. The model proved to be quite satisfactory in explaining most of the basic features of galaxy clustering without serious conflicts with the observed limits on the cosmic background radiation (hereafter CBR) anisotropies. The very difficulty of the model is the general lack of structure on large scales; in particular it is unable to predict large-scale streaming motions (as measured, for instance, by the velocity–velocity correlation) and a cluster–cluster correlation function in agreement with observations. This difficulty is also shown by the cosmic Mach number test, proposed by Ostriker & Suto (1990), which reveals that such a deficiency is independent of the fluctuation amplitude. The reason for this flaw must be ascribed to the fact that structures on any scale are created hierarchically from the bottom: since the only characteristic length of the model is $\lambda_{eq} \approx 13\ (\Omega_0\ h^2)^{-1}$ Mpc, the horizon scale at the equivalence epoch, structures on much larger scales are rare events in Gaussian statistics.

Recently, the observational evidence of large-scale power has been confirmed by the 'bubbly' appearance of the de Lapparent, Geller & Huchra (1988) slice of the CfA catalogue, by the discovery of structures on an unexpectedly large scale, such as the 'Great Wall' (Geller & Huchra 1989), by the analysis of the galaxy angular-correlation function in the APM survey (Maddox *et al.* 1990) and by the amazing results of deep pencil-beam surveys (Broadhurst *et al.* 1990).

A CDM model of Gaussian adiabatic perturbations with primordial spectral index $n < 1$ and/or density parameter $\Omega_0 < 1$, motivated by generalized inflation (Abbott & Wise 1984; Lucchin & Matarrese 1985), seems to be the most

conservative change to the standard scenario able to alleviate the large-scale problem. Such a possibility, investigated by Vittorio, Matarrese & Lucchin (1988), is however restricted by CBR anisotropy limits. Another possibility is to give up the initial scale freedom of the spectrum by introducing *ad hoc* characteristic scales in the primordial perturbations (e.g. Bardeen, Bond & Efstathiou 1987). This is possible in particular inflationary models (e.g. Kofman & Linde 1987; Salopek, Bond & Bardeen 1989; Hodges & Blumenthal 1990) which do not, however, always fulfil a simplicity criterion. Phenomenological models with primordial isocurvature baryon perturbations have also been explored, following a suggestion by Peebles (1987). In its simplest version, however, the model predicts exceedingly high CBR fluctuations (see the discussion by Bond 1990). Moreover, attempts to build up early-Universe models where baryonic perturbations are generated, ended up with inconsistencies (see the discussion by Mollerach 1990). Standard models with Hot Dark Matter (e.g. Centrella *et al.* 1988) do not seem viable candidates for originating structures, due to the '*age of galaxy formation*' problem. A more radical change is certainly to abandon the idea that galaxies originated by a gravitational instability-driven process, as in models where the formation of structures is induced by cosmic strings, explosions, late-time phase transitions and cosmic textures.

Instead, one can consider the unexplored possibility that the statistics of primordial perturbations is non-Gaussian: the purpose of this work is to perform numerical simulations of the large-scale structure of the Universe starting from non-Gaussian initial conditions. Such an assumption, which can implement the CDM scenario, has the advantage of preserving the simplicity of the gravitational-instability picture. Along this line we preliminarily investigated a class of non-correlated non-Gaussian models by N-body simulations, mainly to test the sensitivity of the non-linear clustering process to non-random phases in the initial conditions (Messina *et al.* 1990, hereafter Paper I).

The immediate difficulty one has to face is the wide indeterminacy in assuming non-Gaussian statistics. In the choice of possible classes of models one can, however, follow some simple criteria. Some sort of scale invariance can be considered as a guiding principle, in the same spirit as, in the early seventies, this requirement allowed the selection of the Harrison–Peebles–Zel'dovich spectrum as the most natural one, much before the inflationary paradigm made such a prediction. Another criterion can be that of building up the perturbation process by performing simple non-linear transformations, for instance of multiplicative type, on a Gaussian random field. This procedure can be thought of as a non-trivial generalization of the one leading to the Gaussian statistics from a discrete Bernoulli process via the central limit theorem: a possible statistics obtained this way is the lognormal one which is the prototype for multiplicative processes. One could assume that different physical processes are able to generate this kind of distributions inside the horizon: in any case, at earlier epochs, inflation-generated non-Gaussian perturbations are expected to be of multiplicative type (Matarrese, Ortolan & Lucchin 1989; Kofman *et al.* 1990; Barrow & Coles 1990).

In particular, we have considered three types of multiplicative non-Gaussian statistics, chosen as distributions for the peculiar gravitational potential, $\Phi(x)$, before the inclusion of the CDM transfer function. The first one, that we call the 'convolution' (hereafter C) model, is obtained by convolving two independent Gaussian processes, as originally proposed by Peebles (1983). A second one, the 'lognormal' statistics, is the extreme case of multiplicative distribution which typically arises in hierarchical fragmentation processes; it formally splits in two quite different models. As we shall see in Section 2, a first model, called $\mathrm{LN_p}$, is characterized by positive skewness for the linear mass fluctuation δ_M, i.e. $\langle \delta_M^3 \rangle > 0$, implying that positive fluctuations occur more frequently than negative ones. A second model with negative skewness will be called $\mathrm{LN_n}$. The last one we consider is a chi-squared distribution with one degree of freedom. In this case also two possibilities appear, which we shall call χ_p^2 and χ_n^2, according to the previous criterion. Hereafter, we shall refer to $\mathrm{LN_p}$ and χ_p^2 as *positive* and $\mathrm{LN_n}$ and χ_n^2 as *negative* models. In general, all these models are obtained by performing non-linear transformations on a Gaussian random field $w(x)$. All our distributions are built up in such a way that Φ has power spectrum

$$\mathscr{P}_\Phi(k) = \frac{9}{4}\mathscr{P}_0 k^{-3} T^2(k), \tag{1}$$

where $\mathscr{P}_0(k)$ is the primordial Zel'dovich spectrum of density fluctuations. We take the CDM transfer function (e.g. Davis *et al.* 1985)

$$T(k) = [1 + 1.7\,kl + 9.0(kl)^{3/2} + 1.0(kl)^2]^{-1}, \tag{2}$$

with $l = (\Omega_0 h^2)^{-1}$ Mpc. We consider only models with $\Omega_0 = 1$, so that all lengths in our simulations scale as h^{-2}. Our choice for the spectrum allows a comparison with the evolution of a standard, i.e. Gaussian, CDM (hereafter G) model. We used a particle-mesh code with $N_\mathrm{p} = 64^3$ particles on $N_\mathrm{g} = 64^3$ grid points (see Paper I for details). Computations were performed at the CINECA Centre (Bologna) on a Cray YMP/432 running under UNICOS. A new algorithm for the mass deposition on the grid (Simoncini & Messina 1990) brought an improvement of 25 per cent in CPU time.

The box size of our simulations is $L = 65\ h^{-2}$ Mpc, so that each particle carries a mass $m = 2.94 \times 10^{11}\ h^{-4}\ M_\odot$. After evolving all our models starting from the same amplitude at the initial time, t_i, we analyse their clustering properties from a reference non-linearity time, t_nl, up to the present time, t_0, by different statistical tests. The time t_nl is conventionally fixed when in the Gaussian model non-linear events (i.e. $\delta_M \sim 1$) first occur [this is somewhat earlier than the initial time in the simulations by Davis *et al.* (1985)]; at t_nl the non-Gaussian models preserve most of their initial features, although they already experienced some non-linear evolution in moderately high peaks. The time t_0 occurs, as usual, when the particle two-point function is best fitted by a power law $\xi(r) = (r/r_0)^{-\gamma}$, with $\gamma = 1.8$, in a suitable interval. Fig. 1 shows slices of thickness 1/16 of the box size at t_nl (Fig. 1a) and at t_0 (Fig. 1b), all drawn from the same realization of the underlying Gaussian field $w(\boldsymbol{x})$. The slices at t_nl for lognormal and chi-squared models display the 'intermittency' phenomenon (e.g. Zel'dovich *et al.* 1987), with the occurrence of sporadic high spots where most of the intensity of the random field [$\delta_M(\boldsymbol{x})$ for positive and $-\delta_M(\boldsymbol{x})$ for negative models] is stored, separated by large regions of reduced intensity. Moderately high peaks of the underlying

Gaussian field w are non-linearly magnified by the multiplicative process leading to Φ and thus to δ_M. The slices at the final time t_0 show striking variations among different models which will be quantitatively confirmed by the detailed statistical analysis. The main result will be that both the dynamics of clustering and the present texture are mostly sensitive to the sign of the primordial skewness. Positive models cluster more rapidly showing a lumpy structure with small correlation length; the resulting peculiar velocities are also quite small. Large-scale structures in negative models form late, by the merging of shells surrounding primordial underdense regions, and give rise to a cellular structure with filaments, sheets and large voids; the resulting correlation length and rms bulk motion turn out to be very large. Both the structure and the dynamics of the C model, which has vanishing initial skewness, are quite similar to the standard Gaussian CDM: the multiplicative process here only mixes the phases without producing coherent structures on large scales.

The plan of the paper is as follows. In Section 2 we introduce our non-Gaussian models; in Section 3 we discuss their evolution and present clustering properties. The statistical tests already used in Paper I will not be described in detail. Section 4 contains a discussion of the main results.

2 NON-GAUSSIAN MODELS

We assume that the fundamental quantity is the gravitational-potential fluctuation Φ, this being the typical gauge-invariant (up to a zero-mode) variable whose statistics is fixed by primordial processes, like in inflation. [Our potential is simply related to the quantity Φ_H introduced by Bardeen (1980): $\Phi = -\Phi_H$.] Moreover, emphasis on the gravitational potential as a possible unbiased tracer of the mass distribution has come from the work by Bertschinger & Dekel (1989). Also, the recently proposed 'adhesion' model, which implements the Zel'dovich approximation, draws the skeleton of the large-scale structure from the properties of

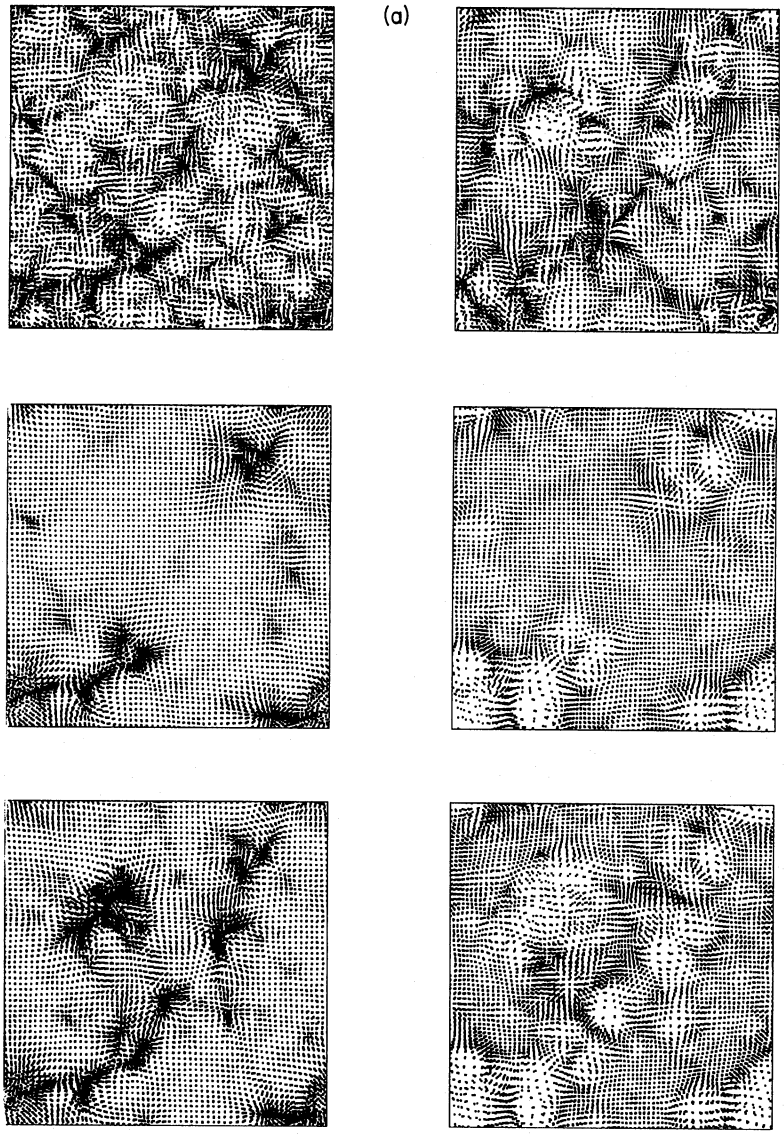

Figure 1. (a) Projected particle positions in slices of depth one-sixteenth of the computational box size at the non-linearity time t_{nl}. The slices refer to the different models: G (top left), C (top right), LN_p (centre left), LN_n (centre right), χ^2_p (bottom left) and χ^2_n (bottom right). (b) The same slices which were selected in (a) are shown at the present time t_0.

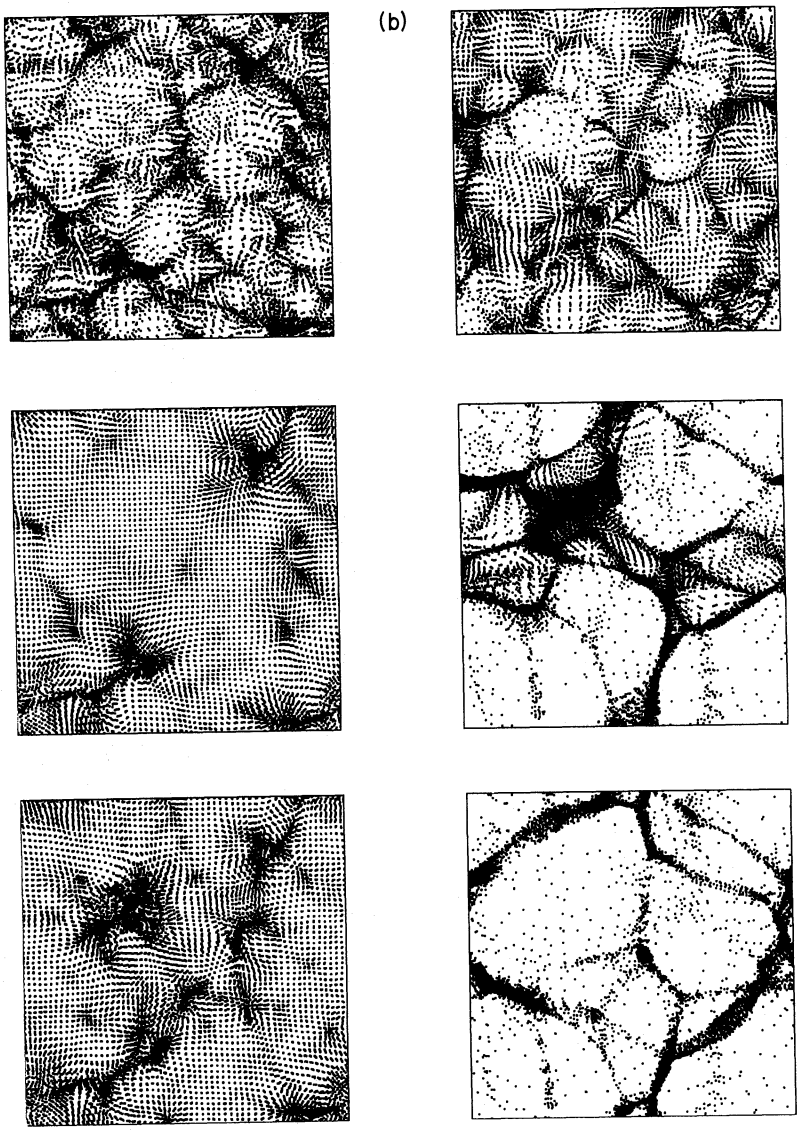

Figure 1 – *continued*

the gravitational potential (e.g. Gurbatov, Saichev & Shandarin 1989). Such a potential can be used to define the phase-space particle distribution $f_z(\boldsymbol{x}, \boldsymbol{p}; t)$ through the Zel'dovich algorithm (as discussed in Paper I),

$$f_z(\boldsymbol{x}, \boldsymbol{p}; t) = \frac{\varrho(t)}{m}\,\delta^3[\boldsymbol{p} + m\nabla_q \Phi(\boldsymbol{q})], \tag{3}$$

where $\varrho(t)$ is the average mass density, m the particle mass, $\boldsymbol{p} = m\,d\boldsymbol{x}/db$ its momentum and $\boldsymbol{q} = x - b(t)\boldsymbol{p}/m$; $b(t)$ is the growing mode of linear perturbations, proportional to the scale factor $a(t)$ in a flat matter-dominated universe. The phase-space distribution completely determines both the mass–density and the peculiar velocity fields before shell crossing. Unlike the density-fluctuation field, the gravitational potential is required neither to have zero mean, since only its gradient is physically meaningful, nor to satisfy the positive-mass constraint. The potential Φ defines the linear mass fluctuation δ_M via the Poisson equation,

$$\delta_M(\boldsymbol{x}, t) = \frac{2}{3\dot{a}^2(t)}\,\nabla_x^2 \Phi(\boldsymbol{x}). \tag{4}$$

A simple consequence of this equation is that $\langle \delta_M \rangle$ consistently vanishes only provided $\Phi(\boldsymbol{x})$ is a stationary random process.

The models we consider are obtained by the following procedure. The gravitational potential is taken as the convolution of a real function $\tau(\boldsymbol{x})$ with a stationary, zero-mean, random field $\varphi(\boldsymbol{x})$:

$$\Phi(\boldsymbol{x}) = \int d^3y\,\tau(\boldsymbol{y} - \boldsymbol{x})\,\varphi(\boldsymbol{y}). \tag{5}$$

The field φ will be related to one or more Gaussian random processes via some non-linear operation, and the function τ will be fixed by its Fourier transform,

$$\tilde{\tau}(\boldsymbol{k}) \equiv \int d^3x e^{-i\boldsymbol{k}\cdot\boldsymbol{x}} \tau(\boldsymbol{x}) = T(k), \tag{6}$$

where $T(k)$ is the transfer function.

Let us now describe the various models in more detail.

2.1 Convolution

This is a model where the random field φ is given by the convolution

$$\varphi(\boldsymbol{x}) = \int d^3y \alpha(\boldsymbol{y}-\boldsymbol{x}) n(\boldsymbol{y}) w(\boldsymbol{y}), \tag{7}$$

where α is a real function, n and w are two independent zero-mean Gaussian fields whose power spectra are

$$\mathscr{P}_n(k) = 1, \tag{8}$$

so that n is white noise [i.e. $\langle n(\boldsymbol{x}) n(\boldsymbol{y})\rangle = \delta^3(\boldsymbol{x}-\boldsymbol{y})$], and

$$\mathscr{P}_w(k) = \frac{2\pi^2 k^{-3}}{\ln(k_M/k_m)} \qquad k_m \le k \le k_M, \tag{9}$$

with $\mathscr{P}_w(k) = 0$ outside this k interval. With such a choice w has unit variance $\langle w^2\rangle = 1$. The white-noise character of n, together with the w normalization implies that the φ auto-correlation function is completely determined by α, independently of the w spectrum. Requiring that Φ has the CDM spectrum implies that $\tilde{\alpha}(\boldsymbol{k}) = (3/2)\mathscr{P}_0^{1/2} k^{-3/2}$. This is essentially the same model proposed by Peebles (1983) and analysed in some detail by Lucchin & Matarrese (1988). They defined it directly for the density fluctuation; the two definitions are, however, equivalent at the linear level. The model turns out to be symmetric against the change $\Phi \to -\Phi$, so that all odd-order correlation functions vanish. The w power spectrum determines, for instance, the form of the connected fourth moment of δ_M (Peebles 1983); the flicker-noise assumption, equation (9), ensures that non-Gaussian features persist up to the largest scale, $\sim 1/k_m$, caused by the w coherence length.

2.2 Lognormal

The second type of models we consider is obtained using the lognormal statistics for φ,

$$\varphi(\boldsymbol{x}) = A[e^{w(\boldsymbol{x})} - \langle e^w\rangle], \tag{10}$$

where w is a zero-mean Gaussian field with unit variance and power spectrum as in equation (9). There is still the freedom in assuming A to be negative ($\mathrm{LN_p}$ model) or positive ($\mathrm{LN_n}$ model). The φ spectrum is then approximately given by

$$\mathscr{P}_\varphi(k) \approx 2\pi^2 e A^2 \frac{k^{-3}}{\ln(k_M/k_m)}, \tag{11}$$

while the gravitational potential Φ has the CDM power spectrum with amplitude $\mathscr{P}_0 \approx 8\pi^2 e A^2/9 \ln(k_M/k_m)$. One would get different lognormal statistics according to the amplitude of w; if $\langle w^2\rangle$ were small the non-Gaussian character of φ would only manifest in rare high peaks; if, on the other hand, $\langle w^2\rangle$ were large, the φ power-spectrum would deviate from flicker noise. It is easy to calculate the three-point function of linear density fluctuations for this model; from it one finds that $\mathrm{LN_p}$ ($\mathrm{LN_n}$) has positive (negative) skewness (hence the names we assigned to these models). The lognormal statistics have been considered in Paper I as a distribution for space-uncorrelated density fluctuations. This model has been analysed in the cosmological context by many authors (e.g. Coles & Jones 1991 and references therein); the most closely related work is the one by Coles (1989) on the peaks of a lognormal mass-density field.

2.3 Chi-squared

The third kind of distribution is obtained by considering a chi-squared statistic with one degree of freedom:

$$\varphi(\boldsymbol{x}) = A[w^2(\boldsymbol{x}) - \langle w^2\rangle], \tag{12}$$

w being a Gaussian fluctuation field with the same power spectrum as equation (9). It can be shown (Lucchin, Matarrese & Ortolan, in preparation) that the φ power spectrum is given by

$$\mathscr{P}_\varphi(k) = \frac{2\pi^2 A^2}{\ln^2(k_M/k_m)} k^{-3}[\beta(k) + 2\ln(1 + k/k_M) - 1], \tag{13}$$

where $\beta(k) = (1 - k/k_m)^2$, for $k_m \le k \le 2k_m$, and $\beta(k) = +2\ln(-1 + k/k_m)$, for $2k_m \le k \ll k_M$. The constant A can be either negative (χ^2_{p} model) or positive (χ^2_{n} model). The names are chosen according to the sign of $\langle \delta_M^3\rangle$, as before. For intermediate scales, the Φ power spectrum is close to the standard CDM one with amplitude $\mathscr{P}_0 \approx 2(4\pi A/3)^2 \ln(k/k_m)/\ln^2(k_M/k_m)$. Chi-squared models have been considered by Coles & Barrow (1987), in connection with the two-dimensional statistics of CBR fluctuations. In the inflationary

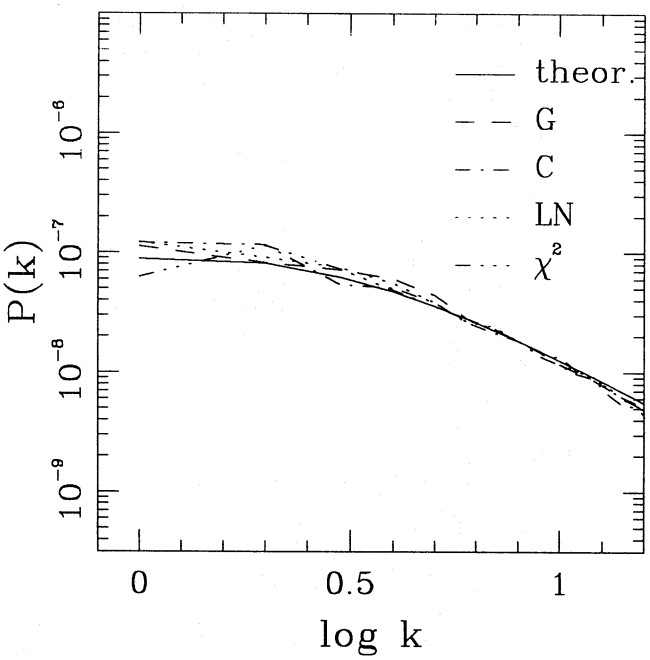

Figure 2. The simulated Cold Dark Matter initial power spectrum $\mathscr{P}(k)$ plotted for the different models versus the theoretical one (solid line). The wavenumber k is normalized in units of $2\pi/L$, where L is the size of the computational box (65 h^{-2} Mpc).

context, Bardeen (unpublished; see also Salopek, Bond & Bardeen 1989) proposed a model where adiabatic perturbations are described by a squared Gaussian process, our χ^2_p, whose w field has a non-scale-free power spectrum.

To get the initial conditions for our simulations, we first generate by standard procedures (e.g. Efstathiou *et al.* 1985) Gaussian realizations in momentum space with the required power spectrum: equations (8) and (9) for C and equation (9) for LN and χ^2 models. The described non-linear transformations are applied in configuration space to get the non-Gaussian φ distributions. The actual gravitational potential Φ, to be processed by the Zel'dovich algorithm, is obtained by further Fourier transformation which allows a straightforward convolution of φ with the transfer function (the C model requires further convolution with the function α).

The previous models are compared with a reference Gaussian one with the CDM spectrum of equation (1). The constant A in χ^2 and LN models can be chosen so that all the power spectra have the same amplitude $\mathscr{P}_0$. The initial amplitude for all the models was lowered to the level where the distribution with the highest positive tail (LN_p in our case) was still free of shell crossings so that the Zel'dovich algorithm could be safely applied. We found that the required amplitude for the linear mass fluctuations is equal to 1/52 of the white-noise level at the Nyquist frequency $k_{Ny}=\pi N_g^{1/3}/L$. In Fig. 2 the computed density-fluctuation spectra at t_i are compared with the theoretical one, $\mathscr{P}(k)=\mathscr{P}_0 kT^2(k)$. Of course, positive- and negative-skewness models have identical spectra.

At the initial time the absolute value of the skewness parameter, $\Sigma\equiv\langle\delta_M^3\rangle/\langle\delta_M^2\rangle^{3/2}$ is of order 2 for LN and χ^2 models, calculated from the particle distribution in bins of side 8 h^{-2} Mpc, i.e. on a scale where the transfer function starts to have reduced effects. With higher resolution, Σ becomes larger for LN and practically constant for the scale-invariant χ^2 models. It is worth noting that the value of Σ does not affect the linearity of the random field. Due to the aggregating action of gravity the skewness is always positive at the end of our simulations: still on the scale of 8 h^{-2} Mpc, G and C have $\Sigma\approx 1.2$, positive models have $\Sigma\approx 3.7$, negative ones reach $\Sigma\approx 0.8$.

Before concluding this section let us make some comments. First of all it should be stressed that, in the general non-Gaussian case, a statistical distribution for $\Phi(\boldsymbol{x})$ does not imply the same distribution for $\delta_M(\boldsymbol{x})$. Moreover, not any statistical distribution can be self-consistently assumed for δ_M. For instance, a chi-squared distribution for δ_M would imply a positive definite two-point function, which is in contrast with large-scale homogeneity, while the same statistics for Φ does not lead to inconsistencies. The assumption implicit in equations (5) and (6) is that the statistics of $\bar{\Phi}(\boldsymbol{k})$ is of primordial origin, i.e. it refers to the time when that fluctuation mode was outside the Hubble radius. Also, the overall sign, which is just a phase, should be fixed by the primordial physical mechanism giving rise to the perturbation field. This statistic is left invariant in the linear regime, independent of the physical processes which modify the k-content of Φ, on every scale not involved in acoustic oscillations. It is worth noting that the flicker-noise choice for the w spectrum, which gives equipartition in Fourier space, is stable (up to small corrections) against the non-linear operation leading to φ, both in χ^2 and LN models.

Both C and χ^2 models represent examples of scale-invariant non-Gaussian statistics (Otto *et al.* 1986; Lucchin & Matarrese 1988). On the other hand, χ^2 and LN statistics belong to the same general class $\varphi(\boldsymbol{x})\propto|1+\alpha^{-1}w(\boldsymbol{x})|^\alpha$; in fact, for $\alpha=2$ and $\langle w^2\rangle^{1/2}\gg 1$, the χ^2 distribution is recovered, while $\alpha\to\infty$ yields the lognormal one (Lucchin, Matarrese & Ortolan, in preparation). For small wave numbers, where $T(k)\approx 1$, the gravitational potential of scale-invariant distributions obeys the scaling law

$$\langle\bar{\Phi}(\mu\boldsymbol{k}_1)\dots\bar{\Phi}(\mu\boldsymbol{k}_N)\rangle\, d^3(\mu k_1)\dots d^3(\mu k_N)\approx\langle\bar{\Phi}(\boldsymbol{k}_1)\dots \times\bar{\Phi}(\boldsymbol{k}_N)\rangle\, d^3k_1\dots d^3k_N, \tag{14}$$

for any N, up to logarithmic corrections owing to the cut-off wave numbers. This gives a straightforwad generalization of the Harrison–Peebles–Zel'dovich scale invariance to non-Gaussian statistics. As a consequence, the particle distribution derived from the Zel'dovich algorithm, before shell crossing, obeys a simple rule: the spatial distribution at time t_2 will appear the same as it was at time t_1 provided that all lengths are rescaled by the factor $\mu=(t_2/t_1)^{1/3}$.

3 EVOLUTION AND CLUSTERING PROPERTIES

As we mentioned in Section 1, the present time is fixed by the slope $\gamma=1.8$ of the particle two-point function in the amplitude interval $0.3\lesssim\xi(r)\lesssim 30$ [in agreement with the choice by Davis *et al.* (1985)]. Fig. 3 shows the correlation function at various expansions. The scale factor is normalized to $a_{nl}=a(t_{nl})$. In Table 1 we report the values of the expansion for our models when the slope is closest to the observed one (this is the present time t_0); the corresponding correlation length r_0, in units of h^{-2} Mpc, and the slope of the correlation function are also reported. The errors represent one standard deviation. Models G and C get the right slope at $a_0=a(t_0)\approx 2.3$. Positive models evolve faster, $a_0\approx 1.65$, determining the noisy appearance of the correlation function. Quite different is the behaviour of negative models, which need a long non-linear evolution, $a_0\approx 7.5$, before reaching the present. Due to the different rates of non-linear evolution, the correlation length turns out to be quite different for the different models. Models G and C have small correlation length. The 'classical' value $r_0=5\ h^{-1}$ Mpc can only be obtained with uncomfortably low values of h: we get $h\approx 0.3$ which represents a relevant flaw for these models [Davis *et al.* (1985) find $h\approx 0.25$ for the standard

Table 1. Model parameters.

Model	a_0	γ	r_0	$R_{V,max}$
G	2.4	1.83 ± 0.02	1.84 ± 0.08	2.12
C	2.2	1.81 ± 0.03	1.80 ± 0.10	2.29
LN_p	1.8	1.90 ± 0.09	1.54 ± 0.14	1.27
LN_n	7.0	1.79 ± 0.01	4.14 ± 0.18	8.95
χ^2_p	1.5	1.88 ± 0.08	1.61 ± 0.15	1.15
χ^2_n	8.0	1.81 ± 0.02	4.04 ± 0.17	9.56

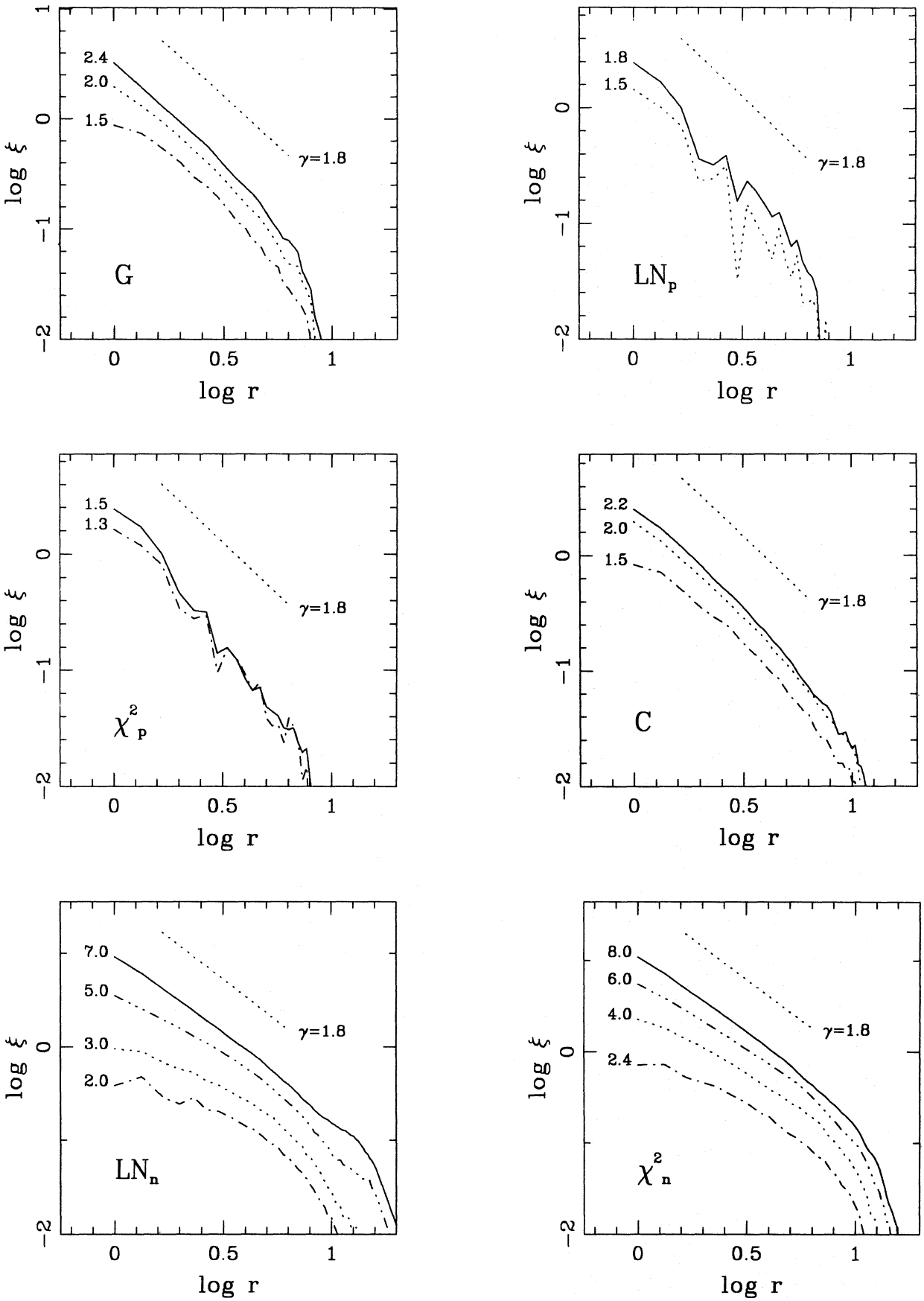

Figure 3. The particle two-point correlation function ξ versus the logarithm of the distance r (in h^{-2} Mpc units) at various expansions for the different models. The observed slope $\gamma = 1.8$ is also shown for reference.

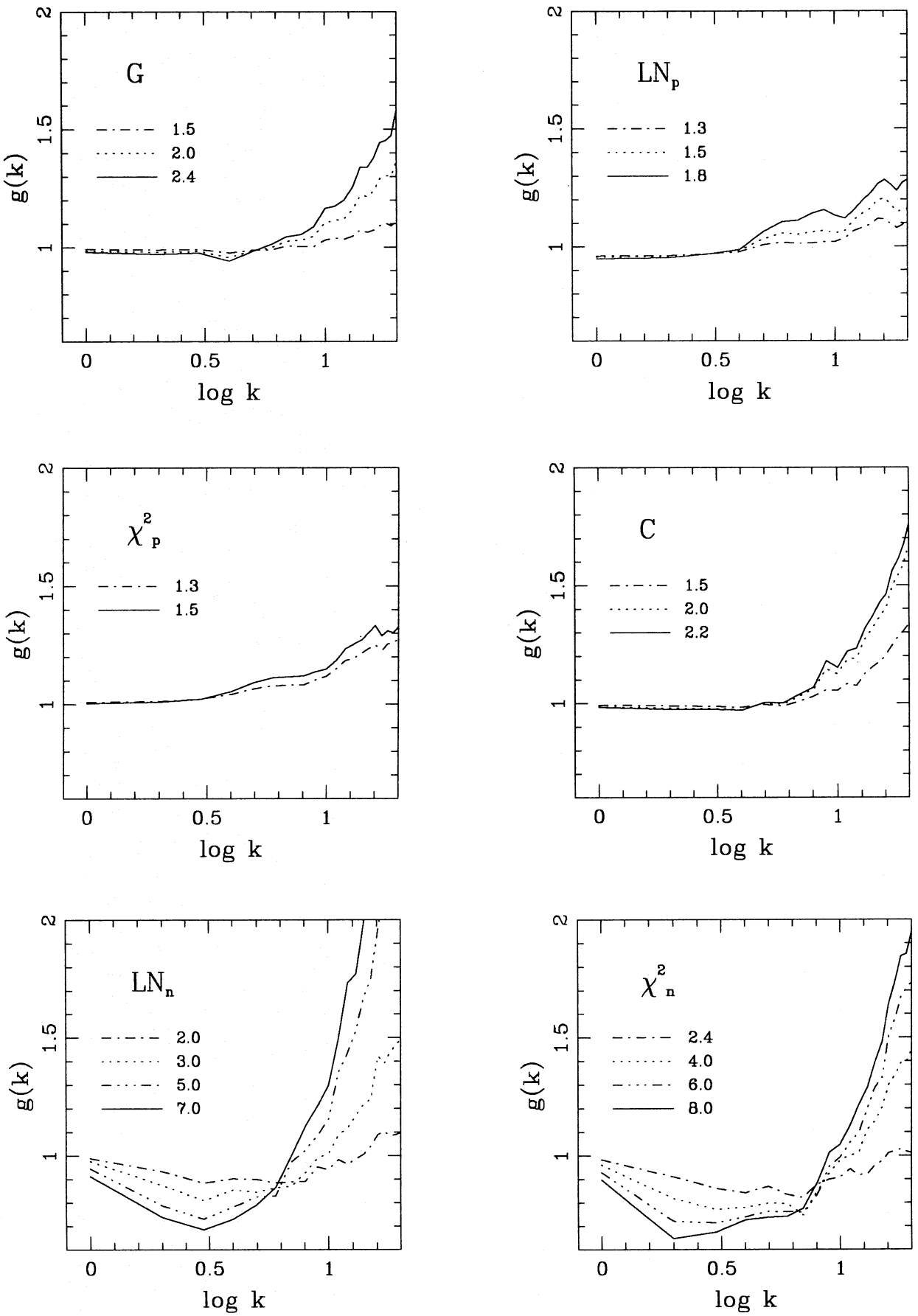

Figure 4. The spectral growth rate $g(k, a)$ at various expansions for the different models. The wave number k is normalized as in Fig. 2.

CDM]. For positive models r_0 is even smaller. In both cases, a substantial biasing would be required. Negative models have enough time to push the non-linearity to larger scales; in this case the classical r_0 value is obtained with $h \approx 0.8$. With $h = 0.5$ the high correlation length of negative models can easily accommodate the recently favoured value $r_0 \approx 7.5\ h^{-1}$ Mpc (de Lapparent, Geller & Huchra 1988).

A possible way to analyse the non-linear dynamics of the models is that of looking at the spectral growth rate

$$g(k, a) \equiv \sqrt{\frac{\mathscr{P}(k, a)\, a_{\rm nl}^2}{\mathscr{P}(k, a_{\rm nl})\, a^2}}, \qquad (15)$$

which gives the evolution of the density-fluctuation power spectrum normalized to its linear growth. In Fig. 4 we plot this function at different epochs versus the wavenumber [the same quantity is plotted in a different way by Suto (1989)]. In a bottom-up scenario $g(k, a)$ deviates sensibly from unity starting from large wavenumbers. We verified that the spectral growth rate for our models is approximately constant from $t_{\rm i}$ to $t_{\rm nl}$ when most of the fluctuations are still in the linear regime. This indicates that $t_{\rm nl}$ roughly represents the onset of non-linearity: $t_{\rm nl}$ occurs 52 expansions after $t_{\rm i}$. All the models show a critical wavelength λ_* below which the growth is more than linear, a signal of hierarchical clustering. The dynamics of small-scale fluctuations is dominated by those existing in lumpy regions, corresponding to a locally closed universe. Such a critical wavelength is $\sim 13\ h^{-1}$ Mpc for the G and C models, somewhat smaller for the negative and larger for the positive ones: λ_* is of the same order as the CDM characteristic scale $\lambda_{\rm eq}$. Above this scale the growth is essentially linear for all but the negative models which display an impressive slowing down in their evolution at large scales: the dynamics of fluctuations in this case is monitored by the large underdense regions, corresponding to a locally open universe. The strong non-linearity of negative models on small scales is to be ascribed to the long evolution after $t_{\rm nl}$: this is expected to produce high-velocity dispersion.

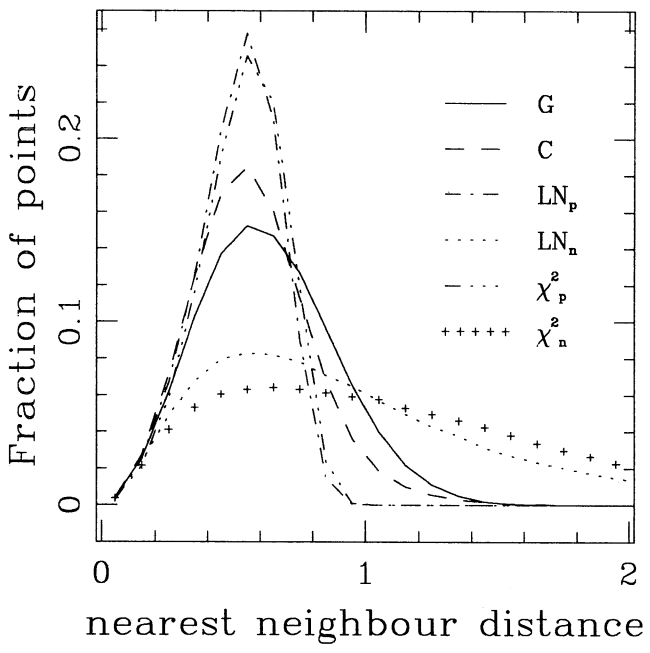

Figure 5. Fraction of grid points whose nearest particle is at the given distance, in units of the mean inter-particle separation $\ell \approx 1.02\ h^{-2}$ Mpc, at the present time t_0.

Most of the features which were shown by the analysis of the spectral growth rate are confirmed by the statistical tests aiming to reveal specific structures such as voids and filaments in the matter distribution.

The last column of Table 1 reports the typical radius $R_{V,\max}$ of the largest void in the simulation at t_0, in units of h^{-2} Mpc, obtained by means of the nearest-neighbour statistics (Ryden & Turner 1984). $R_{V,\max}$ is the maximum distance between the nearest-neighbour particle to a grid point. The whole distribution of such distances is shown in Fig. 5. All the distances in this test are affected by an error of the order of $0.1\ h^{-2}$ Mpc. Once again the models can be grouped in three classes: G and C have voids of size intermediate between positive and negative models. As it is clear from the slices of Fig. 1b, the negative models have the largest voids which formed by the percolation of smaller, initially underdense, regions. It should be stressed, however, that the periodic boundary conditions used in the simulations forbid the presence of voids with dimension comparable to the box size.

The mean contour genus per unit volume $g_{\rm S}$ for our six models is plotted in Fig. 6 at $t_{\rm nl}$ and t_0. The $g_{\rm S}$ curves are obtained using the program by Weinberg (1988). The simulated data have been filtered using a Gaussian window with radius $R_f = 3.5\ h^{-2}$ Mpc [with the Gott *et al.* (1989) notation for the Gaussian filter, $W(\boldsymbol{x}, R_f) = (\pi R_f)^{-3/2} \exp(-|\boldsymbol{x}|^2/R_f^2)$]. For the ease of comparison with the work of Gott *et al.* (1989) we plot $g_{\rm S}$ as a function of the effective relative threshold $\nu_{\rm V}$ defined so that $\mathrm{erfc}(\nu_{\rm V}/\sqrt{2})$ is twice the volume fraction enclosed by the contour where $\delta_M = \nu \langle \delta_M^2 \rangle^{1/2}$. As stressed in Paper I, in the general non-Gaussian case the use of $\nu_{\rm V}$ instead of ν implies a distortion of the real genus curve (see also Coles & Barrow 1987). We also calculated $g_{\rm S}$ as a function of the volume fraction enclosed by each given density contour: in this case more flattened curves result which are not biased by the above distortion. Since the qualitative behaviour ('sponge-like', 'meatball', 'swiss cheese') of the different models is the same as shown in Fig. 6 and since observational data have not yet been processed in terms of such an unbiased variable, we shall not report quantitative results. We plan to return to this point in a future work, considering both numerical simulations and observational data. Because of their lumpiness, positive models easily develop a meatball topology characterized by isolated positive density fluctuations in a connected under-dense sea. The same trend was found for a class of positive-skewness models considered in Paper I. This kind of topology is displayed by a composite sample of galaxies analysed by Gott *et al.* (1989) on a filtering scale of 600 km s^{-1}. Models G and C show the usual sponge-like topology where high- and low-density regions are both inter-connected. Finally, negative models have a swiss cheese (or cellular) topology which is further enhanced by the long non-linear evolution until t_0: voids were surrounded by connected sheets and/or filaments of high density. Although this property may seem in contrast with the claimed meatball topology of the actual galaxy distribution we do not consider this as a flaw of negative models. A preliminary analysis shows that the genus statistics is extremely sensitive to the very definition of galaxies in the simulation. If, for instance, galaxies were

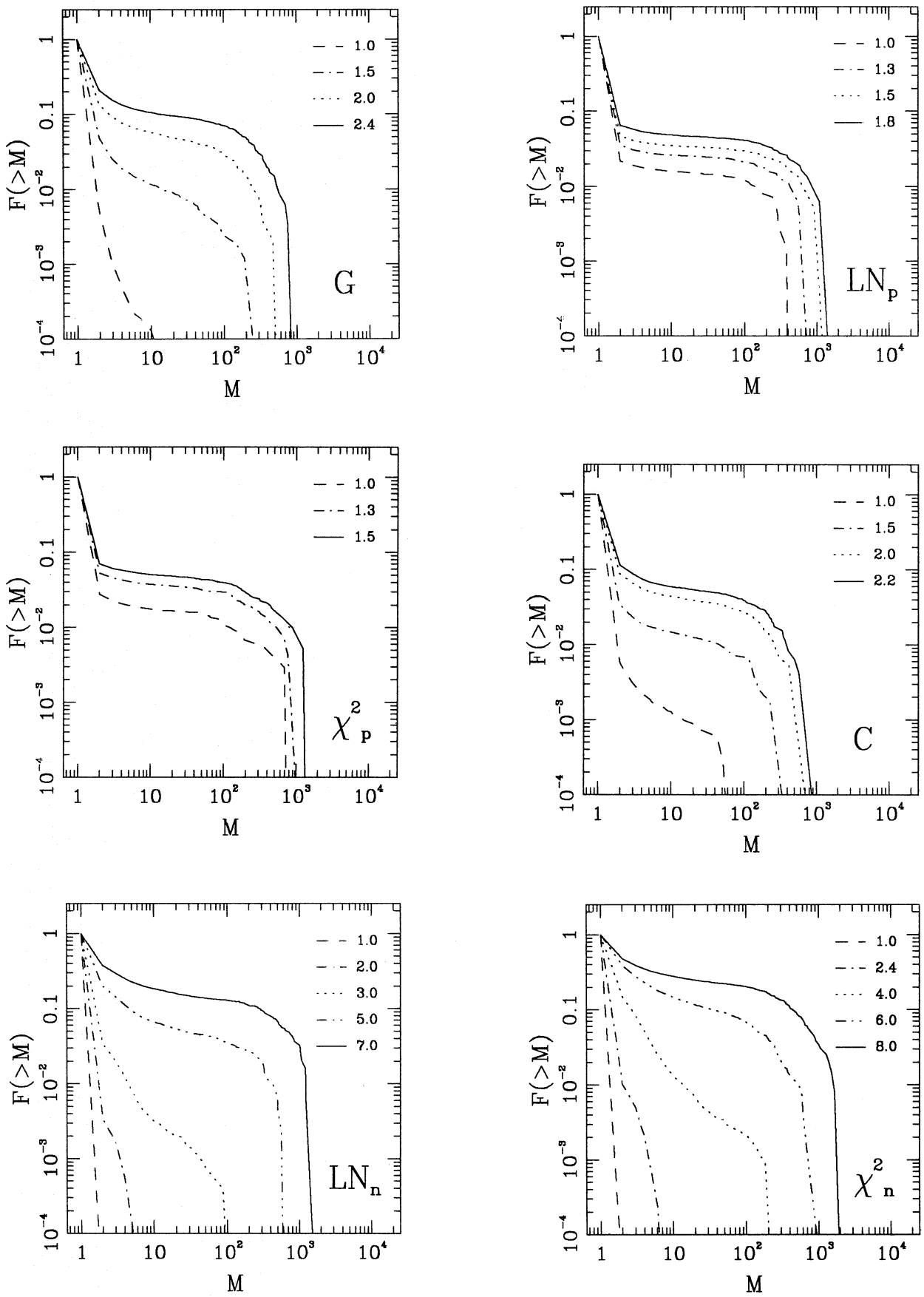

Figure 6. The mean genus density g_S versus the effective relative threshold ν_r, with filtering radius 3.5 h^{-2} Mpc, for the different models. The dashed line refers to t_{nl}, the solid one to t_0.

identified by a suitable 'friends-of-friends' algorithm or by thresholding the mass distribution, the genus curve would result shifted towards the required meatball topology. This point will be considered in greater detail in a future paper where the properties of groups in our N-body simulations will be analysed.

The topology of the different classes of models is also confirmed by the 'contour crossing' statistics (Ryden 1988), although the meatball or swiss cheese tendency of the curves is less pronounced. Quantitative results of this analysis will not be reported here.

The 'quadrupole' statistics introduced by Vishniac (1986) provides a quantitative measure of flattening and elongation in the spatial distribution. This test calculates a function $S(R)$ from the moments of the point distribution in spheres of radius R (for a detailed description see Paper I). Fig. 7 shows a comparison of the curves $\langle S(R)\rangle/\langle S_P(R)\rangle - 1$ evaluated at the present time for the different models (brackets represent average over centres); the estimated errors are of order 10 per cent. These curves measure the amount of 'filamentariness' on the scale R in excess of a purely random process, $\langle S_P\rangle$ being the expected value of $S(R)$ in a Poisson distribution. The results somehow complement the previous one: as it is also clear from the slices of Fig. 1b, negative models are characterized by long filaments which formed, during the non-linear stage, by the connection of smaller ones. Models G and C are very similar and less filamentary than negative ones on all the considered scales. Positive models, as we shall see from the percolation analysis, are dominated by a large number of isolated mass points and have small and rare filaments.

A deep insight on the clustering of the mass points is provided by the cluster analysis. First we consider the percolation curve (Fig. 8) at t_{nl} and t_0. At the onset of the non-linear stage, all the non-Gaussian models percolate less than the Gaussian one: the critical percolation parameter, in units of the comoving mean inter-particle distance $\ell \approx 1.02\ h^{-2}$ Mpc, is $b_c \approx 0.87$ for all but LN_n which has $b_c \approx 0.94$; G percolates at $b_c \approx 0.77$. At the present epoch, thanks to the merging of over-dense structures, negative models percolate more easily ($b_c \approx 0.36$) than G ($b_c \approx 0.53$) and all the remaining non-Gaussian models ($b_c \approx 0.58$). Each determination of b_c is affected by an absolute error ≈ 0.2. It is worth noting that this statistical test is able to discriminate between G and C. This agrees with a result of Paper I that the cluster analysis is very sensitive to detailed non-Gaussian features.

The cluster analysis also allows us to define a cluster catalogue once a suitable value for the linking parameter b is

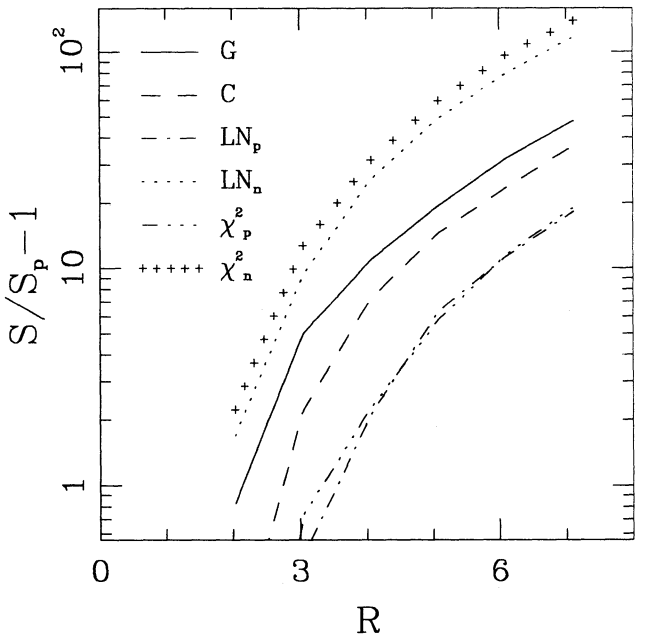

Figure 7. Quadrupole statistics: the function $S/S_P - 1$ is plotted as a function of the radius R, in units of h^{-2} Mpc, at the present time t_0.

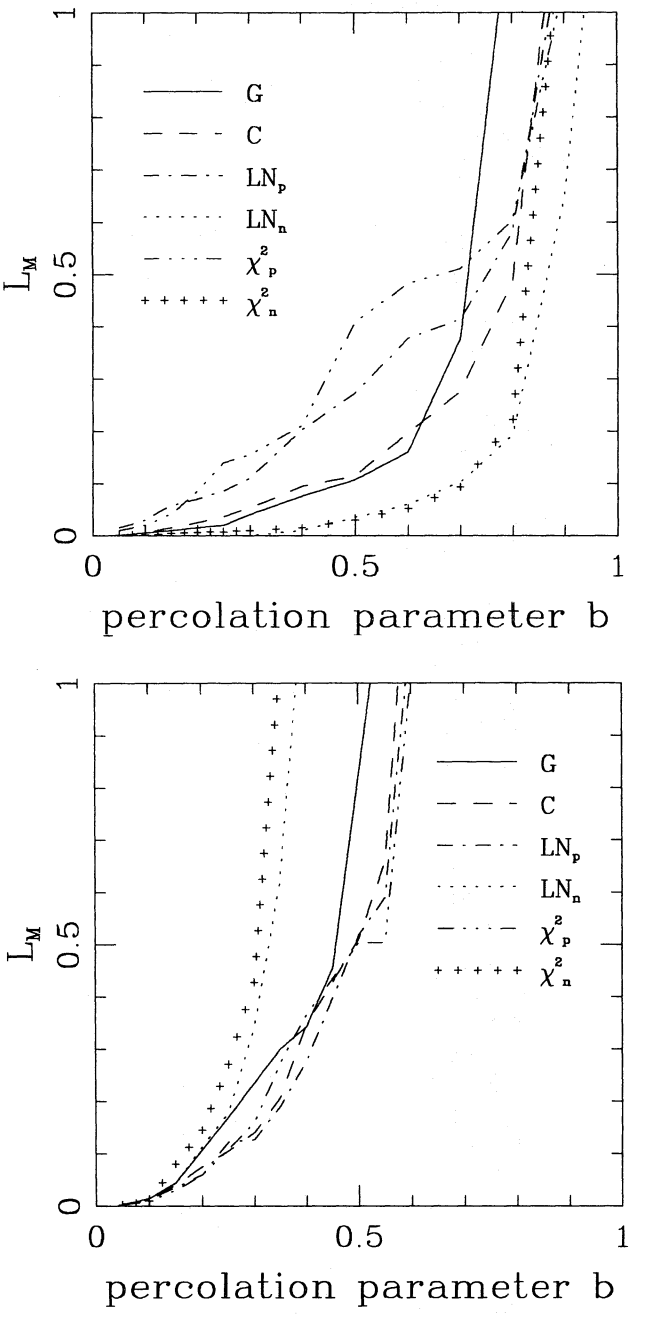

Figure 8. Percolation curve $L_M(b)$ for the different models at t_{nl} (top) and at t_0 (bottom). The percolation parameter b is in units of the mean inter-particle distance $\ell \approx 1.02\ h^{-2}$ Mpc and L_M is in units of the box size L.

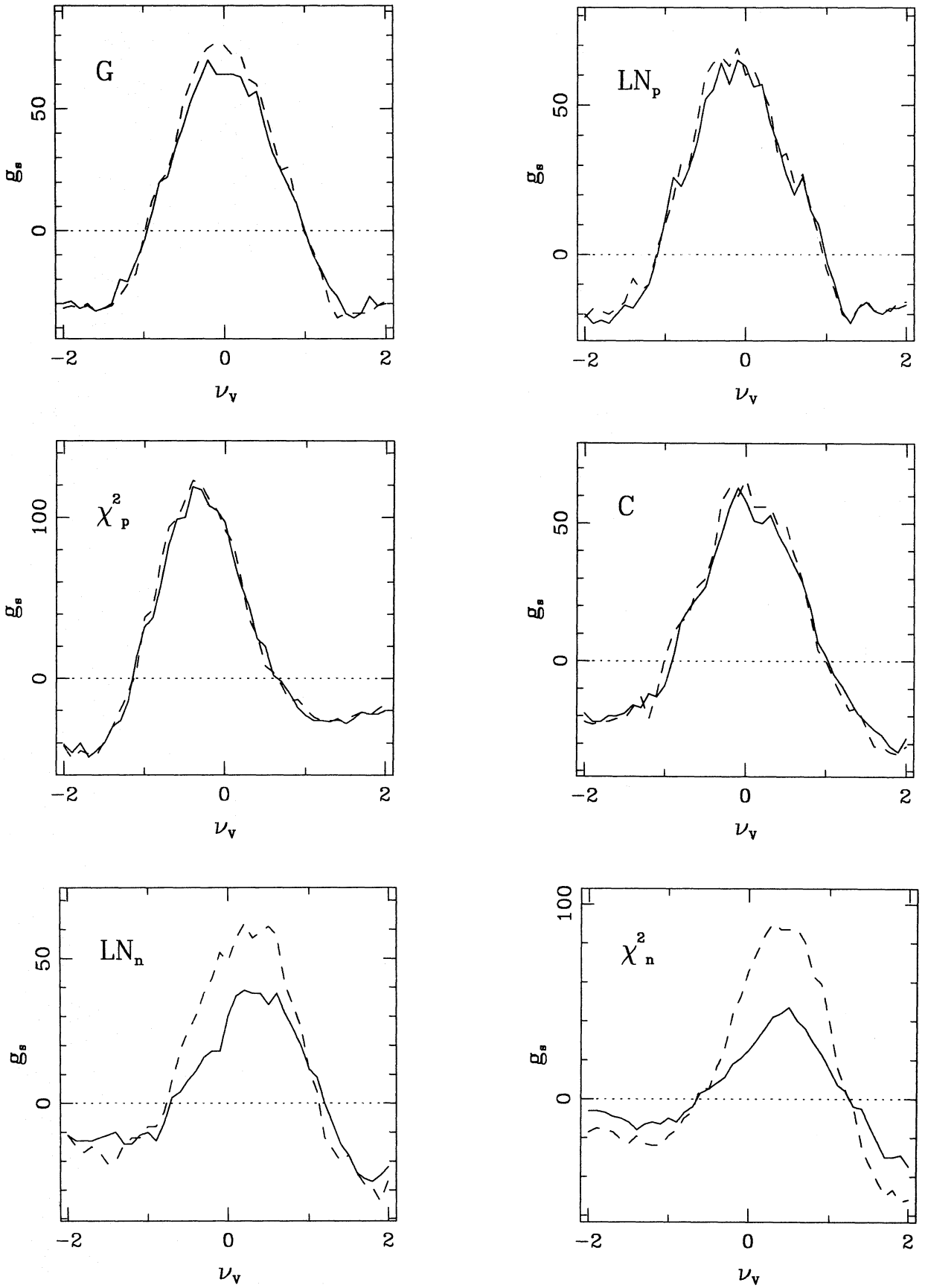

Figure 9. The integrated mass function $F(>M)$ (fraction of mass in clusters with mass larger than M) for a catalogue obtained with linking parameter $b=0.25$, at various expansions. Masses are in units of the particle mass $m=2.94\times10^{11}\ h^{-4}\ M_\odot$.

chosen. We adopt $b=0.25$ (in units of ℓ) which is a reasonable compromise. Lower values would produce a discreteness-dominated catalogue, higher values would give a sample with a few, very massive objects, not suitable for statistical analyses. Fig. 9 shows the evolution of the integrated mass function, the fraction of mass in clusters with mass larger than M,

$$F(>M)=\frac{\Sigma_{j\geq i} j n_j}{\Sigma_j j n_j}, \tag{16}$$

where n_j is the number density of clusters with multiplicity (i.e. number of particles) j and $i\equiv M/m$. Fig. 10 shows the evolution of the characteristic mass of the catalogue

$$M_c = m\frac{\Sigma_j j^2 n_j}{\Sigma_j j n_j}. \tag{17}$$

These quantities display very clearly the different clustering dynamics of positive and negative models. All the models are characterized by some period of self-similar growth, longer for the negative ones, which start aggregating more and more massive clusters only after a period of stagnation, shorter for the positive ones, where the percolation is rapidly catalysed by the large number of initial small lumps. The characteristic mass of negative models is $M_c \approx 3.2\times10^{13}\ h^{-4}\ M_\odot$, much larger than that of both positive and G models, $M_c \approx 0.8\times10^{13}\ h^{-4}\ M_\odot$; C has $M_c \approx 0.5\times10^{13}\ h^{-4}\ M_\odot$. A relevant feature of positive models, revealed by the low-mass tail of $F(>M)$, is the great abundance of isolated objects. This is again a consequence of their lumpy geometry and short non-linear evolution. The self-similar plateau in $F(>M)$, indicating that some high-multiplicity groups already existed at t_{nl}, is related to the characteristic bump in the percolation curve at that time.

Finally, we examine the velocity field. The analysis of galaxy peculiar motions has recently attracted growing attention (e.g. Burstein 1990) and a number of statistical tools have been proposed, such as the velocity correlation function (Groth, Juszkiewicz & Ostriker 1989; Gorsky *et al.* 1989), the velocity dipoles (Kaiser & Lahav 1989) and the cosmic Mach number (Ostriker & Suto 1990). In Paper I we analysed the evolution of the cosmic Mach number for our scale-free models. We found that this test could not discriminate between different initial statistics. Recently, Park (1990) has computed this quantity in a very large-scale CDM simulation. The small size of our simulations does not allow us to obtain reliable results with this test on interesting scales. Nevertheless, we can still derive information about

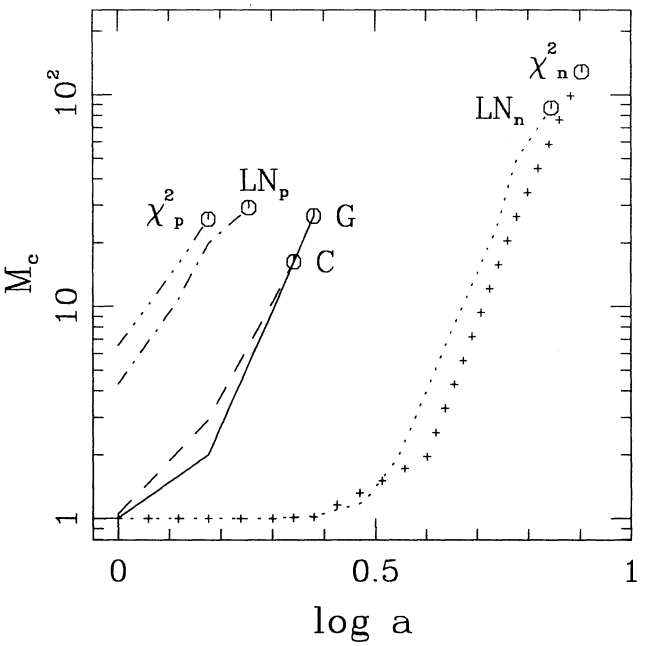

Figure 10. Evolution of the characteristic mass, in units of m, corresponding to $b=0.25$ for the different models. The open circles refer to the values at t_0.

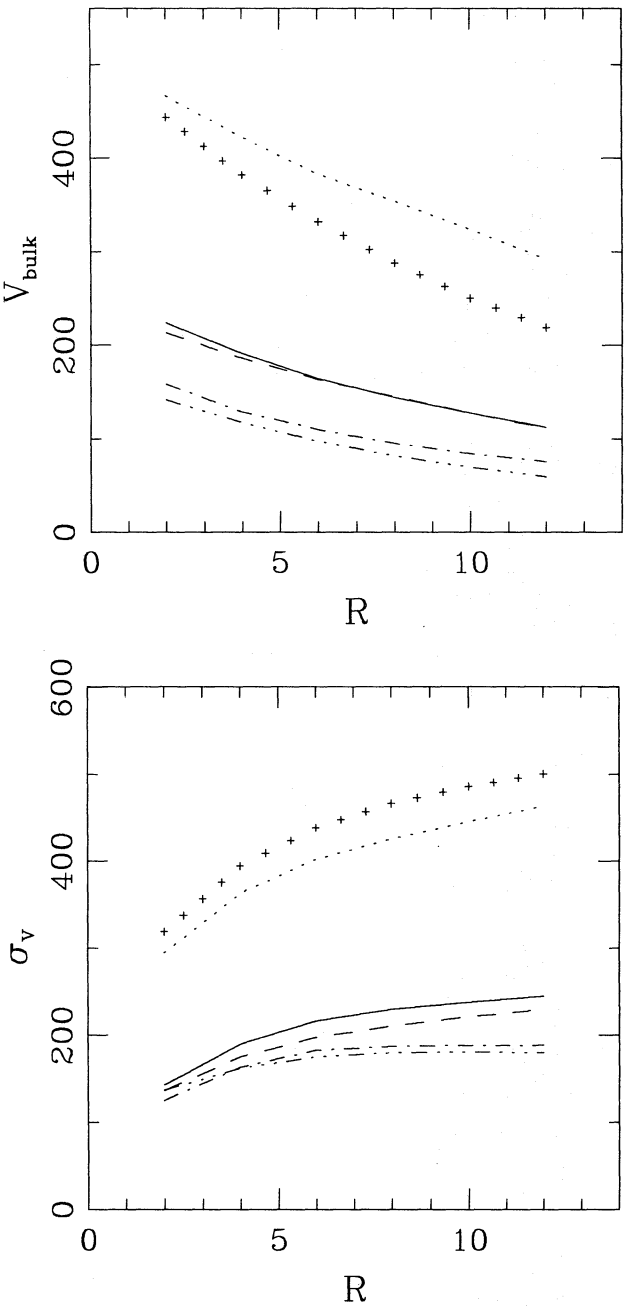

Figure 11. The bulk velocity $V_{bulk}(R)$ (top) and the velocity dispersion $\sigma_V(R)$ (bottom) in units of h^{-1} km s^{-1}, versus the radius R, in units of h^{-2} Mpc, at t_0. The curves refer to the different models as in Fig. 10.

the trend of the peculiar velocity field by analysing directly the bulk velocity $V_{\rm bulk}(R)$ and the velocity dispersion $\sigma_V(R)$ of spherical patches of radius R. Let us define the above quantities. For a patch centred on $\boldsymbol{x}_i$ one can compute the centre-of-mass velocity

$$\boldsymbol{V}(\boldsymbol{x}_i, R) = \frac{1}{N_i(R)} \sum_{|\boldsymbol{x}_j - \boldsymbol{x}_i| \le R} \boldsymbol{V}_j, \tag{18}$$

where $\boldsymbol{x}_j$ and $\boldsymbol{V}_j$ are the position and the peculiar velocity of the j-th particle, respectively; $N_i(R)$ is the number of particles inside that sphere. The residual velocity dispersion of the ith patch is

$$\sigma_V^2(\boldsymbol{x}_i, R) = \frac{1}{N_i(R)} \sum_{|\boldsymbol{x}_j - \boldsymbol{x}_i| \le R} [V_j - V(\boldsymbol{x}_i, R)]^2. \tag{19}$$

The rms quantities $V_{\rm bulk}(R) = \langle |V(\boldsymbol{x}, R)|^2 \rangle^{1/2}$ and $\sigma_V(R) = \langle \sigma_V^2(\boldsymbol{x}, R) \rangle^{1/2}$ can be estimated by averaging over $N_c = 1000$ randomly chosen centres (Suto & Fujita 1989); this procedure introduces errors of order 15 per cent. In Fig. 11 we report the two above quantities, evaluated at t_0, with R ranging from 2 to 12 h^{-2} Mpc. The most relevant result is that negative models are characterized by large bulk motions. We can, for instance, consider a patch of radius 500 km s^{-1}; this is the assumed scale of the Local Group (Lahav, Kaiser & Hoffman 1990), which is endowed with a velocity of 600 km s^{-1} with respect to the CBR rest frame. For $h = 1$, $\mathrm{LN_n}$ has $V_{\rm bulk} \approx 400$ km s^{-1}, while χ_n^2 has $V_{\rm bulk} \approx 360$ km s^{-1}; G, C and positive models all have $V_{\rm bulk} < 200$ km s^{-1}. For $h = 0.5$, negative models have $V_{\rm bulk} \sim 900$ km s^{-1}; all the other ones have $V_{\rm bulk} < 400$ km s^{-1}. Because of the high level of non-linearity on small scales, negative models also have larger velocity dispersion.

4 CONCLUSIONS

In this paper we analysed the evolution of large-scale structures in the Universe starting from non-Gaussian initial perturbations of the gravitational potential in the CDM cosmogony.

Observational data on galaxy clustering require more structure on large scales than given by the standard CDM model: this is the main difficulty of the scenario. Here we exploited the following alternative. Higher-order moments of non-Gaussian statistics can make high peaks in the primordial gravitational potential, corresponding either to overdensities or to voids on large scales, occurring more likely than the random-phase assumption would imply.

The main result of our analysis is that the skewness of the linear mass fluctuation is a strongly discriminating parameter. Compared to the Gaussian model, the convolution one, which has vanishing odd-order correlation functions, presents only modest changes, while the chi-squared and the lognormal statistics, characterized by an absolute value of the skewness parameter of order unity, show relevant differences. When positive and negative models are analysed in the linear regime the topological properties of one are just the 'negative' of the other. The non-linear evolution breaks this symmetry, but the models with the same skewness sign show the same trend in most statistical tests. Many properties of these distributions can be summarized as follows. Negative models have clustering properties similar to the standard biased CDM: structures appear characterized by a high level of connectivity with large voids surrounded by sheets and filaments. On the other hand, the effects of a positive initial skewness are similar to a sort of 'anti-biasing' ($b < 1$) in the standard model.

The actual success of negative models is that all the advantages of the standard biased CDM are obtained without reducing the amplitude of the primordial perturbations. A substantial predominance of primordial underdense regions (negative skewness) is a possible solution to the large-scale problem of the standard CDM scenario. Preserving the bottom-up hierarchical process, negative models succeed in producing a cellular structure with large correlation length and high bulk motions by the slow non-linear process of void merging and disruption of low-density shells. An interactive analysis performed for each run on a graphic work station allowed us to verify that the thick linear structures appearing in the slices of negative models at t_0 typically represent cuts through two-dimensional sheets with the richest clusters occurring at the intersection of filaments.

Although we did not provide any specific mechanism for the generation of perturbations with the assumed statistical distributions, we believe that a number of plausibility conditions, as discussed in Section 1, are fulfilled by our models. It is therefore not impossible that realistic models will be proposed with the required properties. The main lesson we can learn from this analysis is that the lack of large-scale structure in the standard CDM model is not to be ascribed to the gravitational-instability mechanism of structure formation: either the assumed power spectrum or the random-phase hypothesis should be held responsible for this flaw. The cellular structure emerging from the late non-linear evolution of negative models is interestingly similar to the one produced by the so-called 'Voronoi tesselation' (van der Weygaert & Icke 1989; Yoshioka & Ikeuchi 1989), where the formation of large-scale structures is driven by the expansion of voids. In our bottom-up scenario, galaxies are expected to form earlier than the shells surrounding large voids; therefore, the CBR constraints inferred by Coles & Barrow (1990) on Voronoi models do not apply here. The rms 'linear mass fluctuation' of our negative models in a sphere of radius 8 h^{-1} Mpc, obtained by linearly extrapolating the initial variance until t_0, is ≈ 0.9 with $h = 1$ and ≈ 1.6 with $h = 0.5$: a moderate level of biasing is therefore required in order not to exceed CBR anisotropy limits. On the other hand, due to the $\Omega_0 = 1$ assumption, some biasing is needed to consistently define galaxies. In such a case the final time is expected to occur earlier, for a given initial amplitude, than in the unbiased case, therefore reducing the expected amplitude of CBR fluctuations.

The aim of our future work on non-Gaussian models will be: (i) to understand the effects of biasing on the clustering properties of galaxy systems and on the velocity field; in particular, one could wonder whether our positive models can develop coherent structures on large scales; and (ii) to perform larger simulations to discover the size of the largest structure which can be produced by the non-linear evolution of our negative models.

ACKNOWLEDGMENTS

This work has been partially suported by Ministero dell'Università e della Ricerca Scientifica e Tecnologica and by Consiglio Nazionale delle Recerche (Progetto Finalizzato: Sistemi Informatici e Calcolo Parallelo). The staff and the management of the CINECA Computer Center are warmly thanked for their assistance and for allowing the use of computational facilities.

REFERENCES

Abbott, L. F. & Wise, M. B., 1984. *Nucl. Phys.*, **B244,** 541.
Bardeen, J. M., 1980. *Phys. Rev.*, **D22,** 1882.
Bardeen, J. M., Bond, J. R. & Efstathiou, G., 1987. *Astrophys. J.*, **321,** 28.
Barrow, J. D. & Coles, P., 1990. *Mon. Not. R. astr. Soc.*, **244,** 188.
Bertschinger, E. & Dekel, A., 1989. *Astrophys. J.*, **336,** L5.
Bond, J. R., 1990. In: *The Cosmic Microwave Background: 25 years later, Proceedings of the L'Aquila Conference, June 1989,* eds Mandolesi, N. & Vittorio, N., Kluwer, Dordrecht, p. 234.
Broadhurst, T. J., Ellis, R. S., Koo, D. C. & Szalay, A. S., 1990. *Nature,* **343,** 726.
Burstein, D., 1990. *Rep. Prog. Phys.*, **53,** 421.
Centrella, J. M., Gallagher III, J. S., Melott, A. L. & Bushouse, H. A., 1988. *Astrophys. J.*, **333,** 24.
Coles, P., 1989. *Mon. Not. R. astr. Soc.*, **238,** 320.
Coles, P. & Barrow, J. D., 1987. *Mon. Not. R. astr. Soc.*, **228,** 407.
Coles, P. & Barrow, J. D., 1990. *Mon. Not. R. astr. Soc.*, **244,** 557.
Coles, P. & Jones, B., 1991. *Mon. Not. R. astr. Soc.*, **248,** 1.
Davis, M., Efstathiou, G., Frenk, C. S. & White, S. D. M., 1985. *Astrophys. J.*, **292,** 371.
de Lapparent, V., Geller, M. J. & Huchra, J. P., 1988. *Astrophys. J.*, **333,** 44.
Efstathiou, G., Davis, M., Frenk, C. S. & White, S. D. M., 1985. *Astrophys. J. Suppl.*, **57,** 241.
Geller, M. J. & Huchra, J. P., 1989. *Science,* **246,** 897.
Gorski, K., Davis, M., Strauss, M. A., White, S. D. M. & Yahil, A., 1989. *Astrophys. J.*, **344,** 1.
Gott, J. R. *et al.*, 1989. *Astrophys. J.*, **340,** 625.
Groth, E. J., Juszkiewicz, R. & Ostriker, J. P., 1989. *Astrophys. J.*, **346,** 558.
Gurbatov, S. N., Saichev, A. I. & Shandarin, S. F., 1989. *Mon. Not. R. astr. Soc.*, **236,** 385.
Hodges, H. & Blumenthal, G., 1990. Preprint.
Kaiser, N. & Lahav, O., 1989. *Mon. Not. R. astr. Soc.*, **237,** 129.
Kofman, L. & Linde, A., 1987. *Nucl. Phys.*, **B282,** 555.
Kofman, L., Blumenthal, G., Hodges, H. & Primack, J., 1990. In: *Proceedings of the Workshop on Large-Scale Structure and Peculiar Motions in the Universe,* eds Latham, D. W. & da Costa, L. N., ASP Conference Series, in press.
Lahav, O., Kaiser, N. & Hoffman, Y., 1990. *Astrophys. J.*, **352,** 448.
Lucchin, F. & Matarrese, S., 1985. *Phys. Lett.*, **164B,** 282.
Lucchin, F. & Matarrese, S., 1988. *Astrophys. J.*, **330,** 535.
Maddox, S. J., Efstathiou, G., Sutherland, W. J. & Loveday, J., 1990. *Mon. Not. R. astr. Soc.*, **243,** 692.
Matarrese, S., Ortolan, A. & Lucchin, F., 1989. *Phys. Rev.*, **D40,** 290.
Messina, A., Moscardini, L., Lucchin, F. & Matarrese, S., 1990. *Mon. Not. R. astr. Soc.*, **245,** 244 (Paper I).
Mollerach, S., 1990. *Phys. Rev.*, **D42,** 313.
Ostriker, J. P. & Suto, Y., 1990. *Astrophys. J.*, **348,** 378.
Otto, S., Politzer, H. D., Preskill, J. & Wise, M. B., 1986. *Astrophys. J.*, **304,** 62.
Park, C., 1990. *Mon. Not. R. astr. Soc.*, **242.** 59P.
Peebles, P. J. E., 1983. *Astrophys. J.*, **274,** 1.
Peebles, P. J. E., 1987, *Nature,* **327,** 210.
Ryden, B. S., 1988. *Astrophys. J.*, **333,** L41.
Ryden, B. S. & Turner, E. L., 1984. *Astrophys. J.*, **287,** L59.
Salopek, D. S., Bond, J. R. & Bardeen, J. M., 1989. *Phys. Rev.*, **D40,** 1753.
Simoncini, V. & Messina, A., 1990. Preprint.
Suto, Y., 1989. In: *Proceedings of the Workshop on Dark Matter and Structure in the Universe,* p. 129, ed. Sasaki, M., RITP Hiroshima University, Hiroshima.
Suto, Y. & Fujita, M., 1990. *Astrophys. J.*, **360,** 7.
van der Weygaert, R. & Icke, V., 1989. *Astr. Astrophys.*, **213,** 1.
Vishniac, E., 1986. In: *Inner Space/Outer Space,* p. 190, eds Kolb, E. W., Turner, M. S., Olive, K., Seckel, D. & Lindley, D., University of Chicago Press, Chicago.
Vittorio, N., Matarrese, S. & Lucchin, F., 1988. *Astrophys. J.*, **328,** 69.
Weinberg, D. H., 1988. *Publs astr. Soc. Pacif.*, **100,** 1373.
White, S. D. M., Frenk, C. S., Davis, M. & Efstathiou, G., 1987. *Astrophys. J.*, **313,** 505.
Yoshioka, S. & Ikeuchi, S., 1989. *Astrophys. J.*, **341,** 16.
Zel'dovich, Y. B., Molchanov, S. A., Ruzmaichin, A. A. & Sokolov, D. D., 1987. *Sov. Phys. Usp.*, **30,** 5.